

1      Development of a coupled current-wave model  
2      to assess the impact of a hurricane on particle  
3      transport

4      Thomas Dobbelaere, Emmanuel Hanert

5      February 10, 2021

6      **Abstract**

7      In most hydrodynamic model studies, currents and waves are simu-  
8      lated separately. This is especially true for the simulation of passive  
9      drifters, whose trajectories are often computed based solely on cur-  
10     rents. Although this simplification holds for most situations, as the  
11     force exerted by waves on currents can be neglected in fair weather  
12     conditions, it may lead to significant errors in storm conditions, during  
13     which local currents are strongly influenced by wind-generated waves.  
14     In this study, current-wave interactions in heavy-wind conditions are  
15     studied by coupling the unstructured-mesh hydrodynamic model SLIM  
16     with the wave model SWAN in the Florida Reef Tract during Hurricane  
17     Irma (Sep. 2017). This coupled model successfully reproduced both  
18     the observed wave behavior and storm surge during the hurricane.  
19     The modeled currents were then used to simulate the trajectories of  
20     passive drifters during the passage of the hurricane. Our results show  
21     that taking wave force into account induces variations of up 1 m/s  
22     in modelled currents on the continental shelf break as well as in the  
23     vicinity of reefs and islands. Wave-current interactions can therefore  
24     strongly modify the transport of drifting material, such as sediments  
25     and coral larvae, during heavy-wind events. That should in particular  
26     affect connectivity modeling studies since coral mass spawning events  
27     tend to occur during the hurricane season in the Caribbean.

28 **1 Introduction**

29 Individual-based modelling of particulates has been extensively used to  
30 study larval connectivity (Figueiredo et al., 2013; Frys et al., 2020) as larval  
31 dispersal and demographic connectivity cannot be estimated empirically  
32 and genetic similarities are not representative of the flow of individuals re-  
33 quired to maintain a population (Cowen and Sponaugle, 2009). In most  
34 cases, these models are made up of an ocean model simulating flow features  
35 coupled with a Lagrangian tracker including the species-specific life history  
36 characteristics and swimming behavior of the particles. Although some of  
37 these bio-physical models might account for Stokes drift (Fujimura et al.,  
38 2014), wave-induced transport is generally ignored as it is assumed neg-  
39 ligible compared to Eulerian currents. Although this assumption holds for  
40 fair weather conditions, it is not valid in storm conditions, when wind waves  
41 strongly impact currents. Taking storm-induced wave-current interactions  
42 into account in coral connectivity studies in Florida might therefore be of  
43 outmost importance as hurricanes in this region tend to occur during coral  
44 reproduction period (August-September). This was especially true for hur-  
45 rricane Irma, that struck the reefs of the Florida Keys in September 2017.  
46 As hurricanes intensity and frequency are expected to increase with global  
47 warming (REF ?), it is thus critical to assess the impact of wave-induced  
48 forces on simulated larval transport in storm conditions and its influence on  
49 the predictions of classical individual-based bio-physical models.

50 TODO: Wave models and wave-current model coupling ?

51 **2 Methods**

52 **2.1 Wind and atmospheric pressure for Hurricane Irma**

53 In order to capture the wind speed profile of Irma in our model, high-  
54 resolution H\*Wind (Powell et al., 1998) wind fields were used. As these data  
55 represent 1-min averaged wind speeds, we multiplied them by a factor 0.93  
56 to obtain 10-min averaged wind speeds (Harper et al., 2010), more consis-  
57 tent with the time step of our model. Furthermore, H\*Wind wind profiles  
58 did not cover the whole model extent during the hurricane and were thus

59 blended within coarser wind field extracted from ECMWF ERA-5 datasets.  
 60 Pressure fields of Irma were also constructed using ERA-5 data. However,  
 61 the coarse resolution of the data set caused the depression at the center  
 62 of the hurricane to get smoothed out, leading to an underestimation of the  
 63 pressure gradient in our model (see eq. 1). To better capture the central  
 64 depression of Irma, we built a hybrid pressure field using the position and the  
 65 minimal pressure of the core of the hurricane based on its track in the HUR-  
 66 DAT 2 database (Landsea and Franklin, 2013). Based on this information,  
 67 the hybrid pressure field was constructed by combining an idealized Holland  
 68 pressure profile (Lin and Chavas, 2012) within the radius of maximum wind  
 69 speed of Irma (Knaff et al., 2018) with ERA-5 pressure field. The transition  
 70 between from the Holland profile to ECMWF data outside the radius of  
 71 maximum wind speed data was performed using a smooth step function.

## 72 **2.2 Hydrodynamic model**

73 Ocean currents generated during hurricane Irma in the Florida Reef Tract  
 74 (FRT) were modelled using the unstructured-mesh depth-integrated coast  
 75 ocean model SLIM<sup>1</sup>. The model mesh covers an area similar to the model  
 76 extent of Dobbelaere et al. (2020b), that includes the FRT but also the  
 77 Florida Strait and part of the Gulf of Mexico (Figure 1). However, this area  
 78 has been slightly extended northeastward and westward in order to include  
 79 the location of buoys for wave outputs validation. Furthermore, in order to  
 80 withstand potential cell drying due to storm conditions in this study, we used  
 81 the conservative mode of SLIM with wetting-drying, whose equations write:

$$\begin{aligned}
 \frac{\partial H}{\partial t} + \nabla \cdot (\mathbf{U}) &= 0 \\
 \frac{\partial \mathbf{U}}{\partial t} + \nabla \cdot \left( \frac{\mathbf{U}\mathbf{U}}{H} \right) &= -f \mathbf{e}_z \times \mathbf{U} + \alpha g H \nabla(H - h) - \frac{1}{\rho} \nabla p_{\text{atm}} + \frac{1}{\rho} \boldsymbol{\tau}_s \quad (1) \\
 &\quad + \nabla \cdot (\nu \nabla \mathbf{U}) - \frac{C_b}{H^2} |\mathbf{U}| \mathbf{U} + \gamma (\mathbf{U}_* - \mathbf{U})
 \end{aligned}$$

82 where  $H$  is the water column height and  $\mathbf{U}$  is the depth-averaged transport;  
 83  $f$  is the Coriolis coefficient;  $g$  is the gravitational acceleration;  $h$  is the  
 84 bathymetry;  $\alpha$  is a coefficient stating whether the mesh element is wet

---

<sup>1</sup><https://www.slim-ocean.be>

85 ( $\alpha = 1$ ) or dry ( $\alpha = 0$ );  $\nu$  is the viscosity;  $C_b$  is the bottom drag coefficient;  
 86  $\nabla p_{\text{atm}}$  is the atmospheric pressure gradient;  $\tau_s$  is the surface stress due  
 87 to wind; and  $\gamma$  is a relaxation coefficient towards a reference transport  $\mathbf{U}_*$ .  
 88 As in Frys et al. (2020) and Dobbelaere et al. (2020b), SLIM currents were  
 89 relaxed towards HYCOM (Chassignet et al., 2007) in regions where the water  
 90 depth exceeds a given threshold. At very high wind speeds, the white cap is  
 91 blown off the crest of the waves, which generates a layer of droplets that acts  
 92 as a slip layer for the winds at the ocean-atmosphere interface (Holthuijsen  
 93 et al., 2012). This causes a saturation of the wind drag coefficient for strong  
 94 winds (Donelan et al., 2004; Powell et al., 2003). To account for the impact  
 95 of this saturation on the surface wind stress in our model, we implemented  
 96 the wind drag parameterization of Moon et al. (2007).  
 97 The mesh resolution depended only on the distance to coastlines and reefs,  
 98 bathymetry and bathymetry gradient in order to satisfy SWAN refinement  
 99 criterion  $h/A \geq a$ , where  $h$  is the water depth and  $A$  is the element area.  
 100 The mesh was generated using the Python library seamsh<sup>2</sup>, based on the  
 101 the open-source mesh generator GMSH (Geuzaine and Remacle, 2009) and  
 102 is composed of approximately  $7.7 \times 10^5$  elements. The coarsest elements,  
 103 far away from the FRT, had a characteristic length size of about 5 km. Figure  
 104 1 depicts how a 100-m spatial resolution mesh simulated fine-scale details  
 105 of the ocean currents and significant wave height generated by hurricane  
 106 Irma in the Florida Keys.

### 107 2.3 Wave model

108 Waves were modelled using parallel unstructured SWAN (Booij et al., 1999)  
 109 on the same mesh as SLIM. This model solves the action balance equation,  
 110 which reads (Mei, 1989):

$$\frac{\partial N}{\partial t} + \nabla_x \cdot [(\mathbf{c}_g + \mathbf{u})N] + \frac{\partial}{\partial \theta}[c_\theta N] + \frac{\partial}{\partial \sigma}[c_\sigma N] = \frac{S_{in} + S_{ds} + S_{nl}}{\sigma} \quad (2)$$

111 where  $N = E/\sigma$  is the wave action density;  $\theta$  is the wave propagation direc-  
 112 tion;  $\sigma$  is the wave relative frequency;  $\mathbf{c}_g$  is the wave group velocity,  $\mathbf{u}$  is SLIM  
 113 depth-averaged current velocity;  $c_\theta$  and  $c_\sigma$  are the propagation velocities in

---

<sup>2</sup><https://pypi.org/project/seamsh/>

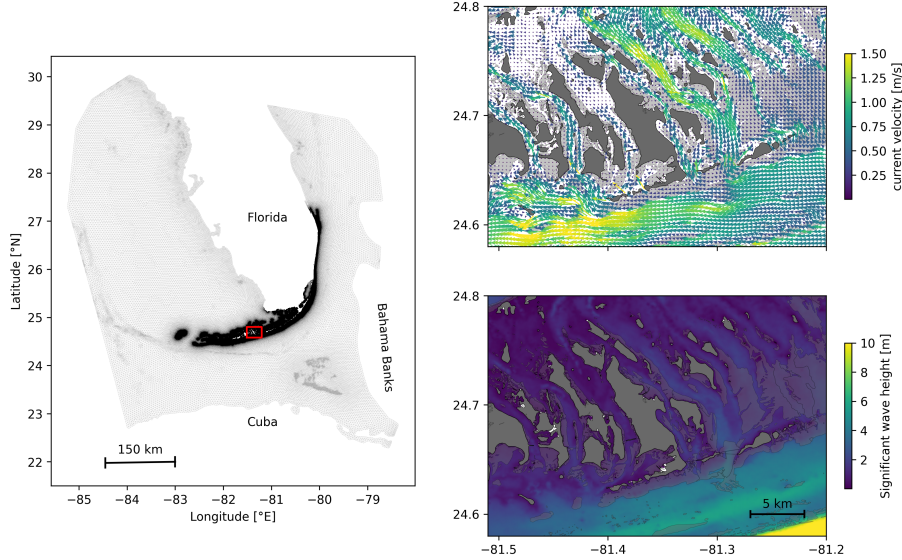


**Fig. 1:** Mesh of the computational domain with snapshots of simulated instantaneous currents and significant wave height on 2017-09-10 at 11:00:00. The mesh resolution ranges from 100 m in the Florida Keys to a maximum of 5 km offshore. Islands are highlighted in dark grey and coral reefs in lighter gray

114 spectral space due to refraction and shifting in frequency due to variations  
 115 in depth and currents; and  $S_{in}$ ,  $S_{ds}$ , and  $S_{nl}$  respectively represent wave  
 116 growth by wind, wave decay and nonlinear transfers of wave energy through  
 117 interactions between triplets and quadruplets. Spectra were discretized with  
 118 48 direction bins and 50 frequency bins logarithmically distributed from 0.3 to  
 119 2 Hz. Exponential wind growth was parameterized using the formulation of  
 120 Janssen (1991), while dissipations by whitecapping and bottom dissipations  
 121 followed the formulations of Komen et al. (1984) and Madsen et al. (1989)  
 122 respectively. Coefficients for exponential wind growth and whitecapping  
 123 parameterizations were based on the results of Siadatmousavi et al. (2011).  
 124 Finally, wave boundary conditions were derived from WAVEWATCH III (Tol-  
 125 man et al., 2009) spectral outputs at buoy locations. Depth-averaged Stokes  
 126 drift was also computed by SWAN using the following formula:

$$\mathbf{u}_s = \int_0^{2\pi} \int_0^{+\infty} \frac{\sigma^3}{h \tanh(2kh)} E(\sigma, \theta) (\cos \theta, \sin \theta) d\sigma d\theta \quad (3)$$

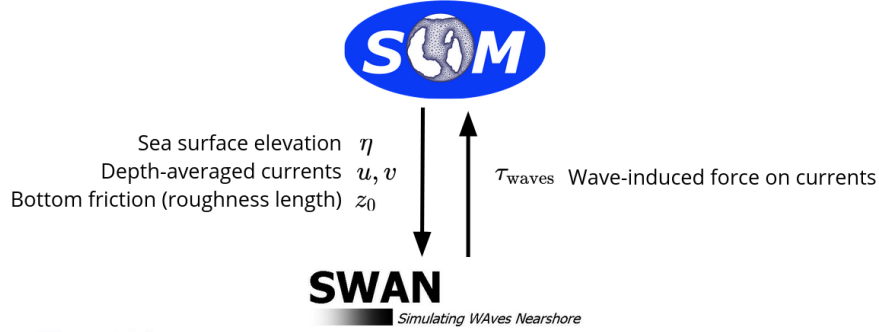


**Fig. 2:** Schematic illustration of the coupled SLIM+SWAN model.

127 where  $k$  is the norm of the wave vector;  $h$  is the water depth; and  $E(\sigma, \theta)$  is  
 128 the wave energy density.

## 129 **2.4 Coupled model**

130 The coupling between SLIM and SWAN is illustrated in Figure 2. The two  
 131 models are run consecutively at each time step. First, SLIM computes the  
 132 sea surface elevation  $\eta$  and depth-averaged current velocity  $\mathbf{u} = (u, v)$ .  
 133 These quantities are transferred to SWAN to update the model water depth  
 134 as well as the second term of equation 2 governing wave energy propagation  
 135 in the geographic space. Moreover, in order for the two model to have con-  
 136 sistent bottom dissipation parameterizations, SLIM bottom drag coefficient is  
 137 transformed into a roughness length  $z_0$  following the methodology of Dietrich  
 138 et al. (2011). This roughness length is then converted into Madsen's bottom  
 139 dissipation term in SWAN. SWAN then produces the wave-induced force on  
 140 current  $\tau_{\text{wave}}$  by computing the wave radiation stress gradient. This quantity  
 141 is used to update the value of the surface stress  $\tau_s$  in equation 1, that now  
 142 becomes the sum of wind and wave-induced forces  $\tau_s = \tau_{\text{wind}} + \tau_{\text{wave}}$ .

## 143 **2.5 Comparison of particle trajectories**

144 To assess the impact of the wave coupling on the modelled currents dur-  
 145 ing hurricane Irma, we compared the trajectories of virtual particles driven  
 146 by currents produced by SLIM alone and SLIM+SWAN simulations in the  
 147 Florida Keys. First, we identified the areas where the differences between

148 the modelled currents were the largest. Then, we determined the potential  
149 origination regions of particles reaching these areas on the passage of the  
150 hurricane through the Florida Keys using backtracking methods (Dobbelaeere  
151 et al., 2020a). These regions are highlighted by the 4 release regions of Fig.  
152 7. Finally, particles were released from these four regions and advected by  
153 currents produced by the coupled and uncoupled models. At each time step,  
154 the center of mass of the modelled particle clouds were computed. The dis-  
155 tance between these centers of mass was used as a measure of the impact  
156 of the wind-generated wave coupling on the modelled current in the Florida  
157 Keys during hurricane Irma. This comparison was performed with 3 sets  
158 of currents: the currents modelled by uncoupled SLIM (SLIM); the currents  
159 modelled by coupled SLIM+SWAN (SLIM+SWAN); and the SLIM+SWAN  
160 currents with depth-averaged Stokes drift (SLIM+SWAN+Stokes).

### 161 **3 Results**

#### 162 **3.1 Validation**

163 Comparisons of the H\*Wind wind and hybrid pressure fields with station  
164 measurements at Vaca Key are shown in Fig. 3. The observed pressure  
165 at the station is well reproduced by the reconstructed hybrid pressure field.  
166 H\*Wind profile agree well with field measurements as well despite a slight  
167 overestimation of the peak wind speed.

168 **QUESTION: Should I use quantitative results such as RMSE ?**

169 To validate the hydrodynamic outputs of the coupled wave-current model,  
170 the computed sea surface elevation was compared with tide gauge measure-  
171 ments on the Eastern and Western coasts of Florida as well as in the Florida  
172 Keys. Figure 4 shows a good fit between simulated and measured elevation  
173 at all stations, where the model succeeds in reproducing the observed tide  
174 surge caused by the passage of the Irma. Modelled currents were validated  
175 against ADCP data at moorings C10, C12 and C13, respectively located at  
176 the 25, 50, and 50 m isobaths of the inner Florida shelf (Liu et al., 2020).  
177 Measured and modelled depth-averaged currents at station C10 are shown  
178 in Fig. 4. The current speed and direction during the hurricane agree well  
179 with observations.

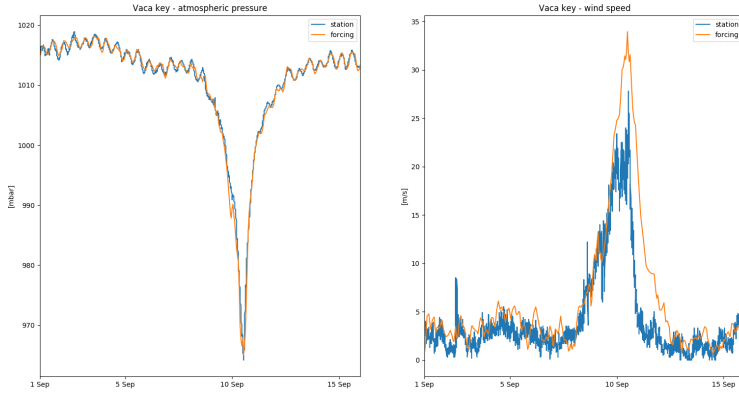


**Fig. 3:** The atmospheric forcings have been validated with meteorological station observations at Vaca Key. The reconstructed atmospheric pressure and wind speed agree well with field measurements.

180 The wave parameters computed by the coupled model were validated  
 181 against field measurements as well. Validation data was extracted from four  
 182 buoys, two in the Eastern coast Florida and two in the inner shelf. Results  
 183 of Fig. 5 show that the model reproduces correctly the timing and ampli-  
 184 tude of the significant wave height peak during the hurricane for all four  
 185 stations. Modelled wave period and direction are in good agreement with  
 186 measurement as well, as shown for station 42036.

### 187 3.2 Impact of waves

188 The impact of hurricane-induced wave-current interactions is first evaluated  
 189 by computing the norm of the maximal difference in current velocity between  
 190 uncoupled SLIM and coupled SLIM+SWAN model runs during the passage  
 191 of Irma through the Florida Keys (from 2017-09-07 to 2017-09-13). Figure  
 192 6 shows that differences in modelled currents are stronger on the shelf  
 193 break and over coral reefs. These results highlight the significant impact  
 194 of wave-induced forces, that can yield differences of up to 1 m/s during the  
 195 hurricane, with stronger currents being obtained with SLIM+SWAN. This  
 196 suggests that neglecting wave-current interactions during Irma would results  
 197 in a significant underestimation of transport over reefs.

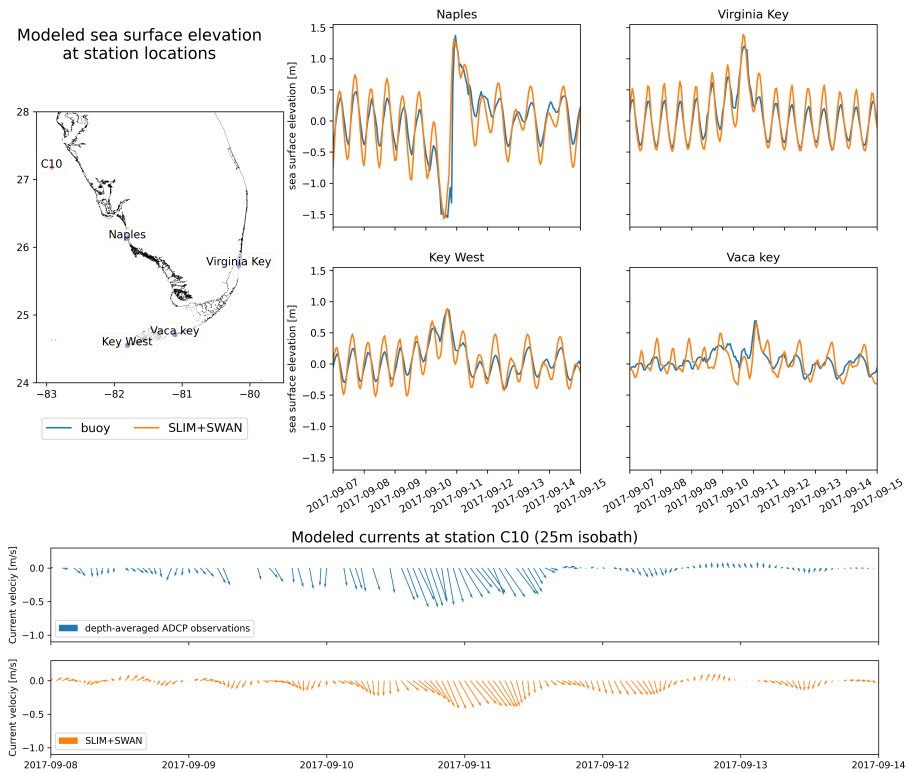


**Fig. 4:** The sea-surface elevation produced by the coupled wave-current model agrees with SSE and current velocity observations at different stations. The fit is particularly good in the Florida Keys and in Naples, on the inner Florida shelf. The coupled model currents have been validated against current meter data on the inner Florida shelf. The current speed and direction during the hurricane agrees well with the observations.

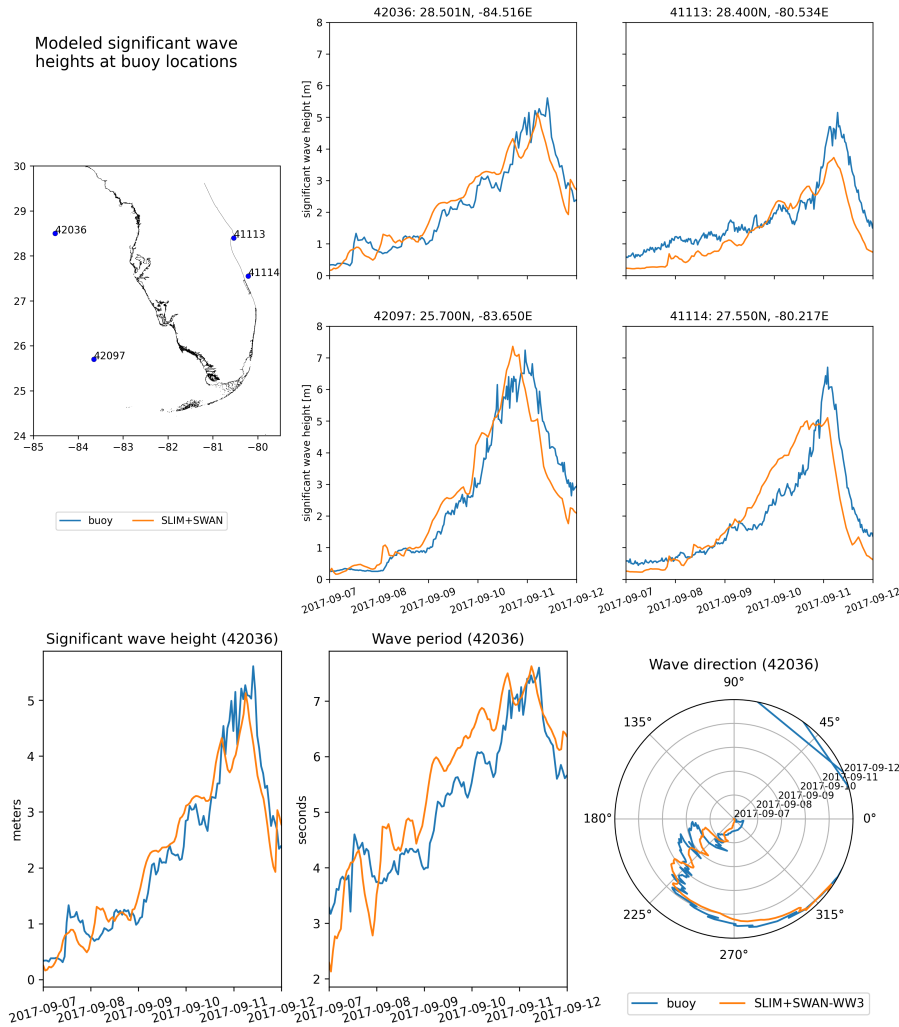


**Fig. 5:** The significant wave height produced by the coupled model has been compared to buoy measurements at 4 different stations. The timing and amplitude of the peak during the hurricane is correctly reproduced for all stations. For station 42036, the period and direction of the waves also agree well with observations

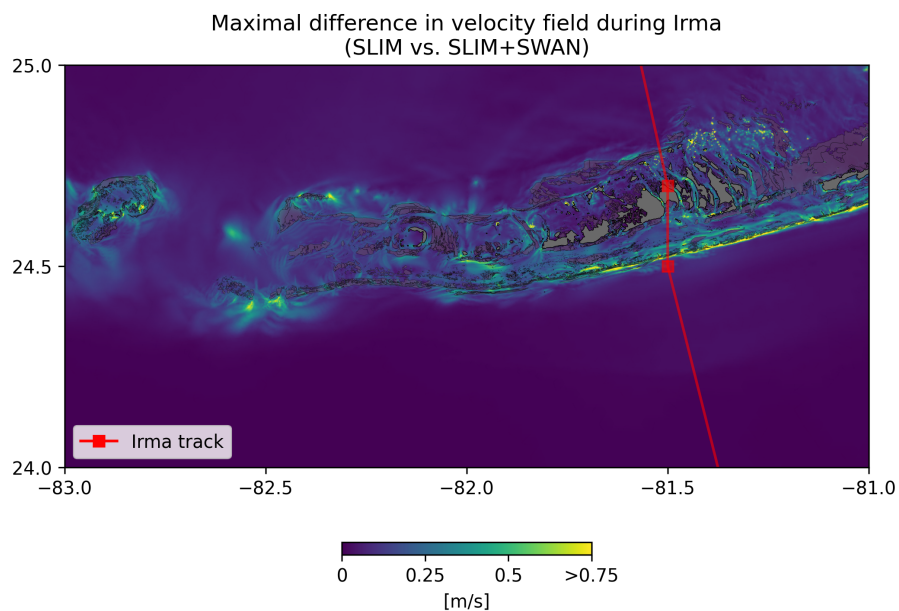


**Fig. 6:** Maximum of the difference between SLIM and SLIM+SWAN currents speed between 2017-09-07 00:00:00 and 2017-09-13 00:00:00. The difference between the coupled and uncoupled model, which represents the effect of the wave-induced stress, can yield differences of 0.5 m/s in the simulated currents during the passage of the hurricane. SLIM+SWAN currents velocities are larger than the currents modeled by SLIM alone. Islands are highlighted in dark grey and coral reefs in lighter grey

198 To quantify the impact of these differences in velocity fields on the modelled  
199 trajectories of passive drifters such as coral larvae, we then tracked virtual  
200 particles advected by SLIM, SLIM+SWAN and SLIM+SWAN+Stokes cur-  
201 rents. Comparison of SLIM and SLIM+SWAN+Stokes trajectories are shown  
202 in Fig. 7. Differences between the modelled trajectories are negligible before  
203 the passage of the hurricanes in the Florida Keys. Then, distance between  
204 the centers of mass of the particles abruptly increase to up to tens of kilo-  
205 meters as Irma gets through the Keys to finally stabilize after the passage  
206 of the hurricane. These results support the assumption that wave-induced  
207 transport is negligible compared to advection by Eulerian currents in fair  
208 whether conditions. However, ignoring waves in storm conditions could  
209 result in significant inaccuracies in modelled trajectories, as illustrated in  
210 the case of release region 2 in Fig. 7. Particles advected by the currents  
211 of the coupled model tend to remain on the shelf while particles advected  
212 by SLIM alone are mostly transported along the shelf break. Although not  
213 shown in this paper, comparison of SLIM and SLIM+SWAN trajectories were  
214 conducted as well. The evolution of the distance between centers of mass  
215 of the particle clouds showed similar trends while yielding smaller values.  
216 Modelled maximal depth-averaged Stokes drift reached up to 0.2 m/s during  
217 the passage of Irma through the Florida Keys. This suggests that both the  
218 impact of wave-induced force on Eulerian currents and Stokes drift should be  
219 taken into account while modelling particle transport under storm conditions.

## 220 **4 Discussion and conclusions**

221 Impact of waves on coral connectivity

222 Ability of wave model to correctly capture gradient in significant wave height  
223 due to current-waves interactions under tropical cyclones depends on:

- 224 • Spatial (10km → 5km) and spectral (36 dir. → 48 dir.) resolution  
225 (Hegermiller et al., 2019)
- 226 • Directional spreading of incident waves (Villas Bôas et al., 2020)

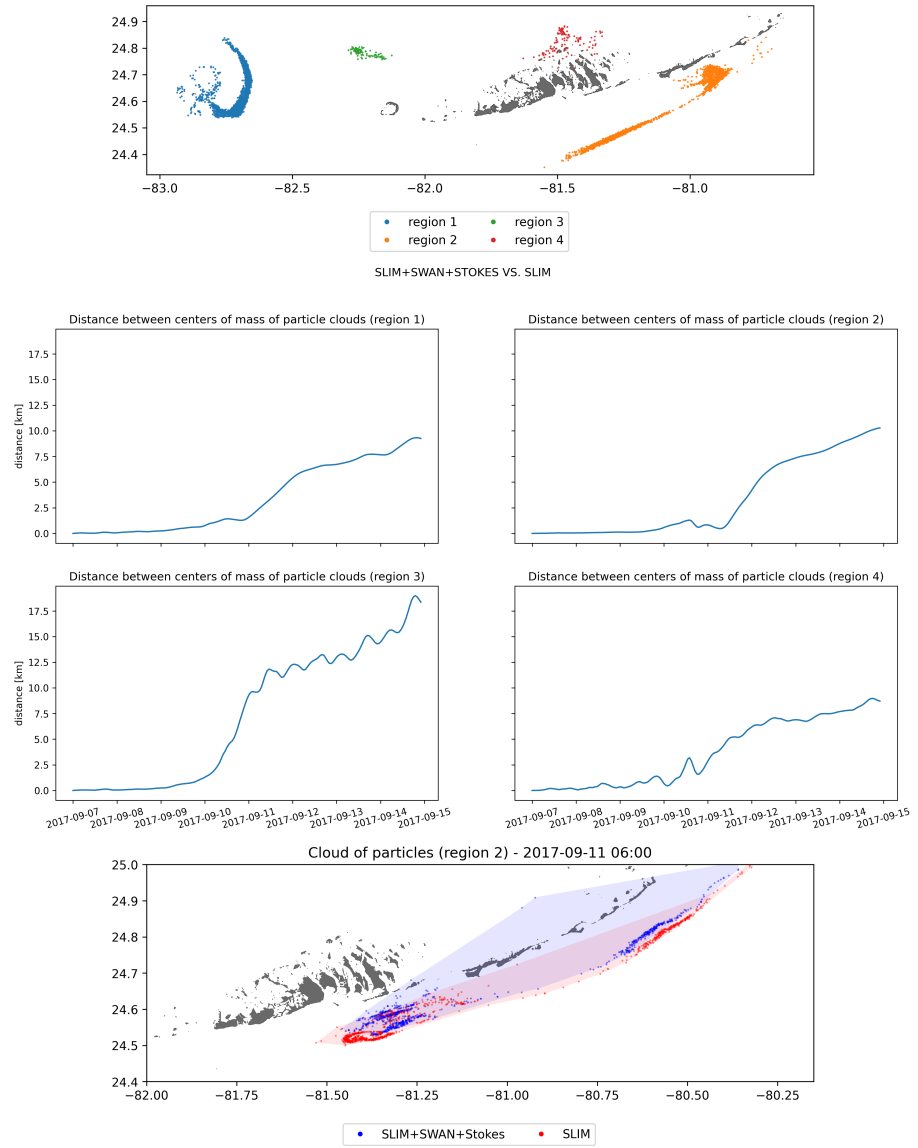


**Fig. 7:** Comparison of passive drifters trajectories with SLIM+SWAN+Stokes drift vs. SLIM alone. A snapshot of the positions of the particles released from region 2 is shown after the passage of Irma in the Florida Keys. Particles advected by the currents of the coupled model tend to remain on the shelf while particles advected by SLIM alone are mostly transported along the shelf break

## **227 Conflict of Interest Statement**

228 The authors declare that the research was conducted in the absence of any  
229 commercial or financial relationships that could be construed as a potential  
230 conflict of interest.

## **231 Author Contributions**

### **232 Funding**

### **233 Acknowledgments**

234 Computational resources were provided by the Consortium des Équipements  
235 de Calcul Intensif (CÉCI), funded by the F.R.S.-FNRS under Grant No. 2.5020.11.  
236 Thomas Dobbelaere is a PhD student supported by the Fund for Research  
237 training in Industry and Agriculture (FRIA/FNRS).

## **238 Supplementary Material**

239 The Supplementary Material for this article is attached to the submitted  
240 document.

## **241 References**

- 242 Booij, N., Ris, R. C., and Holthuijsen, L. H. (1999). A third-generation wave  
243 model for coastal regions: 1. Model description and validation. *Journal*  
244 *of geophysical research: Oceans*, 104(C4):7649–7666.
- 245 Chassignet, E. P., Hurlburt, H. E., Smedstad, O. M., Halliwell, G. R., Hogan,  
246 P. J., Wallcraft, A. J., Baraille, R., and Bleck, R. (2007). The HYCOM  
247 (hybrid coordinate ocean model) data assimilative system. *Journal of*  
248 *Marine Systems*, 65(1-4):60–83.

- 249 Cowen, R. K. and Sponaugle, S. (2009). Larval dispersal and marine  
250 population connectivity.
- 251 Dietrich, J., Westerink, J., Kennedy, A., Smith, J., Jensen, R., Zijlema, M.,  
252 Holthuijsen, L., Dawson, C., Luettich, R., Powell, M., et al. (2011).  
253 Hurricane gustav (2008) waves and storm surge: Hindcast, synoptic  
254 analysis, and validation in southern Louisiana. *Monthly Weather Review*,  
255 139(8):2488–2522.
- 256 Dobbelaere, T., Muller, E., Gramer, L., Holstein, D., and Hanert, E. (2020a).  
257 Report on the potential origin of the SCTLD in the Florida Reef Tract.  
258 Available online at: [https://floridadep.gov/rcp/coral/documents/  
259 report-potential-origin-sctld-florida-reef-tract](https://floridadep.gov/rcp/coral/documents/report-potential-origin-sctld-florida-reef-tract).
- 260 Dobbelaere, T., Muller, E. M., Gramer, L. J., Holstein, D. M., and Hanert, E.  
261 (2020b). Coupled epidemic-hydrodynamic modeling to understand the  
262 spread of a deadly coral disease in Florida. *Frontiers in Marine Science*,  
263 7:1016.
- 264 Donelan, M., Haus, B., Reul, N., Plant, W., Stiassnie, M., Gruber, H., Brown,  
265 O., and Saltzman, E. (2004). On the limiting aerodynamic roughness of  
266 the ocean in very strong winds. *Geophysical Research Letters*, 31(18).
- 267 Figueiredo, J., Baird, A. H., and Connolly, S. R. (2013). Synthesizing larval  
268 competence dynamics and reef-scale retention reveals a high potential  
269 for self-recruitment in corals. *Ecology*, 94(3):650–659.
- 270 Frys, C., Saint-Amand, A., Le Hénaff, M., Figueiredo, J., Kuba, A., Walker, B.,  
271 Lambrechts, J., Vallaeyns, V., Vincent, D., and Hanert, E. (2020). Fine-  
272 scale coral connectivity pathways in the Florida Reef Tract: implications  
273 for conservation and restoration. *Frontiers in Marine Science*, 7:312.
- 274 Fujimura, A. G., Reniers, A. J., Paris, C. B., Shanks, A. L., MacMahan, J. H.,  
275 and Morgan, S. G. (2014). Numerical simulations of larval transport into  
276 a rip-channeled surf zone. *Limnology and Oceanography*, 59(4):1434–  
277 1447.
- 278 Geuzaine, C. and Remacle, J.-F. (2009). Gmsh: A 3-d finite element mesh  
279 generator with built-in pre-and post-processing facilities. *International  
280 journal for numerical methods in engineering*, 79(11):1309–1331.

- 281 Harper, B., Kepert, J., and Ginger, J. (2010). *Guidelines for converting*  
282 *between various wind averaging periods in tropical cyclone conditions.*  
283 Citeseer.
- 284 Hegermiller, C. A., Warner, J. C., Olabarrieta, M., and Sherwood, C. R.  
285 (2019). Wave-current interaction between Hurricane Matthew wave  
286 fields and the Gulf Stream. *Journal of Physical Oceanography*,  
287 49(11):2883–2900.
- 288 Holthuijsen, L. H., Powell, M. D., and Pietrzak, J. D. (2012). Wind and waves  
289 in extreme hurricanes. *Journal of Geophysical Research: Oceans*,  
290 117(C9).
- 291 Janssen, P. A. (1991). Quasi-linear theory of wind-wave generation applied  
292 to wave forecasting. *Journal of physical oceanography*, 21(11):1631–  
293 1642.
- 294 Knaff, J. A., Sampson, C. R., and Musgrave, K. D. (2018). Statistical tropi-  
295 cal cyclone wind radii prediction using climatology and persistence:  
296 Updates for the western North Pacific. *Weather and Forecasting*,  
297 33(4):1093–1098.
- 298 Komen, G., Hasselmann, S., and Hasselmann, K. (1984). On the exis-  
299 tence of a fully developed wind-sea spectrum. *Journal of physical*  
300 *oceanography*, 14(8):1271–1285.
- 301 Landsea, C. W. and Franklin, J. L. (2013). Atlantic hurricane database un-  
302 certainty and presentation of a new database format. *Monthly Weather*  
303 *Review*, 141(10):3576–3592.
- 304 Lin, N. and Chavas, D. (2012). On hurricane parametric wind and appli-  
305 cations in storm surge modeling. *Journal of Geophysical Research:*  
306 *Atmospheres*, 117(D9).
- 307 Liu, Y., Weisberg, R. H., and Zheng, L. (2020). Impacts of hurricane Irma  
308 on the circulation and transport in Florida Bay and the Charlotte Harbor  
309 estuary. *Estuaries and Coasts*, 43(5):1194–1216.
- 310 Madsen, O. S., Poon, Y.-K., and Gruber, H. C. (1989). Spectral wave  
311 attenuation by bottom friction: Theory. In *Coastal Engineering 1988*,  
312 pages 492–504.

- 313 Mei, C. C. (1989). *The applied dynamics of ocean surface waves*, volume 1.  
314 World scientific.
- 315 Moon, I.-J., Ginis, I., Hara, T., and Thomas, B. (2007). A physics-based  
316 parameterization of air–sea momentum flux at high wind speeds and  
317 its impact on hurricane intensity predictions. *Monthly weather review*,  
318 135(8):2869–2878.
- 319 Powell, M. D., Houston, S. H., Amat, L. R., and Morisseau-Leroy, N. (1998).  
320 The HRD real-time hurricane wind analysis system. *Journal of Wind  
321 Engineering and Industrial Aerodynamics*, 77:53–64.
- 322 Powell, M. D., Vickery, P. J., and Reinhold, T. A. (2003). Reduced drag coeffi-  
323 cient for high wind speeds in tropical cyclones. *Nature*, 422(6929):279–  
324 283.
- 325 Siadatmousavi, S. M., Jose, F., and Stone, G. (2011). Evaluation of two WAM  
326 white capping parameterizations using parallel unstructured SWAN  
327 with application to the Northern Gulf of Mexico, USA. *Applied Ocean  
328 Research*, 33(1):23–30.
- 329 Tolman, H. L. et al. (2009). User manual and system documentation of  
330 WAVEWATCH III TM version 3.14. *Technical note, MMAB Contribution*,  
331 276:220.
- 332 Villas Bôas, A. B., Cornuelle, B. D., Mazloff, M. R., Gille, S. T., and Arduin,  
333 F. (2020). Wave–current interactions at meso-and submesoscales:  
334 Insights from idealized numerical simulations. *Journal of Physical  
335 Oceanography*, 50(12):3483–3500.